Multi-vector Matching Deformation Measurement Method

Zhaoqiang Gao
Southeast University
Nanjing, China
Jiangsu Institute of Automation
Lianyungang, China
gao0511@163.com

Jiazhou He
Jiangsu Institute of Automation
Lianyungang, China
18036676276@189.cn

Heng Zhang
Jiangsu Institute of Automation
Lianyungang, China
516163730@qq.com

***Abstract*—This paper introduces a novel multi-vector matching deformation measurement method designed to enhance the stability of deformation measurements in static environments by incorporating specific force observations. The approach effectively measures shift deformation and extends the deformation measurement range by integrating with the velocity matching equation. Furthermore, we propose a conversion model that addresses angular deformation and shift deformation, offering a solution for measuring shift deformation in environments where comparison force observations may not be straightforward. Real inertial navigation experiments conducted in a laboratory setting demonstrate the method's capability to measure deformation in static environments while simultaneously capturing shift deformation. The results illustrate the method's effectiveness in practical deformation measurement scenarios.**

Keywords—Inertial Matching, Hull Deformation, Multi-Vector Matching, Kalman Filter, Deformation Measurement

I. INTRODUCTION

Modern large-scale combat vessels, including amphibious assault ships and aircraft carriers, are outfitted with a spectrum of precision detection tools, such as radar, optoelectronics, vision systems, and sophisticated weaponry like artillery, missiles, and torpedoes. Carrier-based aircraft, such as drones and ship-borne helicopters, further enhance the comprehensive capabilities of these vessels. Ensuring the optimal functionality of these shipboard systems mandates the provision of precise and consistent attitude information [1]. Typically, ships are equipped with high-precision inertial navigation devices or platform compasses strategically positioned at the platform's center or swing center, serving as the primary reference for accurate navigation data. During the construction or maintenance phases of a ship, the positional relationship and attitude conversion between each shipboard equipment and the main reference can be measured [2]. This data, referred to as the attitude transformation matrix, facilitates the conversion of the attitude provided by the main reference into the attitude of the shipboard equipment [3].

However, the previously mentioned approach relies on the assumption of the constancy of the attitude transformation matrix. In real-world scenarios, environmental changes, such as variations in load, wave impacts, external forces, and temperature, can induce angular rotations of the ship's hull and displacement-induced shift deformations [4]. Consequently, the attitude transformation matrix experiences corresponding changes, leading to attitude disturbances that may impact the performance of shipboard equipment, potentially resulting in failure. Therefore, the key to achieving a unified attitude for the entire ship lies in measuring hull deformation and correcting the attitude transformation matrix to provide precise and consistent attitude information for each shipboard equipment [5].

Hull deformation can be categorized into shift deformation and angular deformation based on its form. Shift deformation involves the linear displacement of the hull, which can stretch or contract in the three axes, while angular deformation pertains to the angular displacement of the hull in three axial directions. Typically, when the hull undergoes deformation, both angular and shift deformations occur concurrently [6]. Shift deformation primarily influences the translation transformation within the attitude transformation matrix. Even a minor positional error can impact the safe landing of carrier-based aircraft. Therefore, considering the influence of shift deformation is crucial during takeoff and landing operations [7]. On the other hand, angular deformation predominantly affects the rotational transformation in the attitude transformation matrix. Errors resulting from angular deformation escalate with the extension of detection or weapon strike distances. Even a slight angular deformation can lead to a significant error at longer distances, thereby affecting detection and weapon strike accuracy [8].

In the pursuit of measuring the dynamic deformation of a ship's hull, researchers have proposed an array of real-time measurement methods employing high-precision sensors, such as optical measurement [9], GPS measurement [10], and inertial matching measurement [11]. The inertial matching measurement method, currently a research focal point, exhibits high precision, excellent real-time performance, and user-friendly attributes [12]. Originating from the work of the Russian scholar Mochalov [13], this method involves installing Laser Gyroscope Units (LGUs) at two ship positions. Mochalov measured relative angular deformation based on the gyro outputs of these LGUs, modeling hull deformation as a second-order Markov process. The Kalman filter method is then applied to derive accurate relative deformation, termed the angular velocity matching deformation measurement method. However, due to challenges in determining deformation model parameters, accurately describing hull deformation becomes difficult. Additionally, the angular velocity matching measurement equation presents non-homogeneous issues, leading to suboptimal measurement outcomes in static environments and susceptibility to divergence [11].

Addressing the parameter determination challenge, Wu investigated online identification methods, enhancing parameter accuracy and stability to some extent [14]. Wu also explored utilizing the Bernoulli-Euler beam model as a simplified hull deformation model to improve measurement stability [15]. Similarly, Xu employed a multi-model approach to enhance hull deformation model adaptability and augment the stability of angular velocity matching deformation measurement [16]. Nonetheless, the selection of model parameters and determination of individual model weights remain formidable challenges.

Recognizing the non-homogeneous nature of the angular velocity matching measurement equation under static conditions, Li introduced an accelerometer to improve the stability of the angular velocity matching measurement method [17]. Additionally, Ma proposed that increasing

specific force observations could enhance the stability of the angular velocity matching measurement method [18]. However, augmenting specific force observations introduces the shift deformation variable, leading to diminished deformation measurement efficacy under static conditions.

This paper addresses the limited robustness of the angular velocity matching measurement method in static conditions and its inability to measure shift deformation. To overcome these shortcomings, we propose a multi-vector-based inertial matching measurement method. The multi-vector inertial matching deformation measurement method employs joint matching of angular velocity, attitude array, velocity, and specific force to simultaneously measure angular and shift deformation. Furthermore, we investigate and analyze the relationship between angular deformation and shift deformation. The derived relationship equation enhances the stability of the inertial matching measurement method under static conditions.

The structure of this article is organized as follows: the second chapter details the derivation of the multi-vector inertia matching equation; the third chapter analyzes the relationship between angular deformation and shift deformation; the fourth chapter constructs the Kalman filter equation based on multi-vector inertia matching; in the fifth chapter, we conduct design simulation experiments and physical tests to verify the method's feasibility, followed by a discussion of the results; and finally, the conclusion of this paper is presented in the sixth chapter.

II. MULTI-VECTOR INERTIAL MATCHING MEASUREMENT EQUATION

The coordinate systems used in this paper are shown in Fig.1, mainly including the earth-centered inertial coordinate system (i-frame), the earth-centered ground-fixed coordinate system (e-frame), the main inertial navigation coordinate system (m-frame) and the slave inertial navigation coordinate system (s-frame).

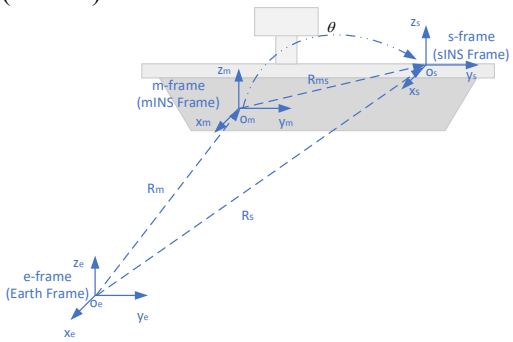

Fig. 1. Coordinate system definition

The coordinate origin of the i-frame is the center of mass of the earth O, the z-axis is the rotation axis of the earth and points to the North Pole, the x-axis points to the vernal equinox in the equatorial plane, the y-axis, z-axes and the x-axis form a right-handed orthogonal coordinate system. The measurement values of inertial devices (gyroscopes, accelerometers) are based on the i-frame, and measure the angular motion parameters and linear motion parameters of the carrier relative to the inertial space.

The coordinate origin of the e-frame is the center of mass of the earth O, the x-axis extends through the intersection of the prime meridian (0 degrees longitude) and the equator, the z-axis extends through the North Pole (that is, coincides with the earth's rotation axis), the y-axis, z-axis and the x-axis form a right hand Coordinate system, passing through the equator and 90 degrees longitude. The e-frame is fixedly connected with the earth, and the angular motion of the e-frame relative to the inertial coordinate system is the angular velocity of the earth's rotation.

The m-frame is the coordinate system of MINS (Master Inertial Navigation System) on the ship, and its coordinate origin is the swing center O_m, the x-axis points to the starboard side of the ship, the y-axis points to the heading direction of the ship, the z-axis points to the sky, the distance vector from the center of the earth is R_m, from O pointing to O_m.

The s-frame is the coordinate system of SINS(Slave Inertial Navigation System) on the ship, and its coordinate origin is a key position on the deck of the ship O_s, the x-axis points to the starboard side of the ship, the y-axis points to the heading direction of the ship, and the z-axis completes the right-hand coordinate system, pointing to the direction of the sky, and the distance vector from the center of the earth is R_s, from O pointing to O_s.

The MINS can measure the angular velocity ω_{im}^m and specific force ω_{im}^m at the position of the MINS, and the SINS can measure the angular velocity ω_{is}^s and specific force f_s^s at the position of the SINS.

A. *Specific force matching equation*

The relationship between vector R_m, R_s and R_{ms}:

$$R_s = R_m + R_{ms} \tag{1}$$

Under the i-frame, (1) can be expressed as:

$$R_s^i = R_m^i + R_{ms}^i = R_m^i + C_m^i R_{ms}^m \tag{2}$$

Where C_m^i is the attitude transformation matrix from m-frame to i-frame in (1), and its time differential can be expressed as:

$$\dot{C}_m^i = C_m^i [\omega_{im}^m \times] \tag{3}$$

Where ω_{im}^m is the projection of the main inertial angular velocity under the m-frame, $[\omega_{im}^m \times]$ is the antisymmetric matrix of ω_{im}^m.

The time derivative of (2) is:

$$\begin{aligned} \dot{R}_s^i &= \dot{R}_m^i + \dot{C}_m^i R_{ms}^m + C_m^i \dot{R}_{ms}^m \\ &= \dot{R}_m^i + C_m^i [\omega_{im}^m \times] R_{ms}^m + C_m^i \dot{R}_{ms}^m \end{aligned} \tag{4}$$

Time differentiation of (4) is:

$$\begin{aligned}\ddot{R}_s^i &= \ddot{R}_m^i + \dot{C}_m^i[\omega_{im}^m\times]R_{ms}^m + C_m^i[\dot{\omega}_{im}^m\times]R_{ms}^m + \\ &C_m^i[\omega_{im}^m\times]\dot{R}_{ms}^m \quad + \dot{C}_m^i\dot{R}_{ms}^m + C_m^i\ddot{R}_{ms}^m \\ &= \ddot{R}_m^i + C_m^i[\omega_{im}^m\times][\omega_{im}^m\times]R_{ms}^m + C_m^i[\dot{\omega}_{im}^m\times]R_{ms}^m \\ &+C_m^i[\omega_{im}^m\times]\dot{R}_{ms}^m \quad + C_m^i[\omega_{im}^m\times]\dot{R}_{ms}^m + C_m^i\ddot{R}_{ms}^m \\ &= \ddot{R}_m^i + C_m^i[\omega_{im}^m\times][\omega_{im}^m\times]R_{ms}^m + C_m^i[\dot{\omega}_{im}^m\times]R_{ms}^m \\ &+2C_m^i[\omega_{im}^m\times]\dot{R}_{ms}^m + C_m^i\ddot{R}_{ms}^m\end{aligned} \tag{5}$$

Where the $\ddot{R}_m^i$ and $\ddot{R}_s^i$ is the acceleration of the master inertial navigation and the slave inertial navigation, and the specific force f_m^m and f_s^s measured by the MINS and the SINS includes the gravity g_m and g_s at the two positions. Since the master inertial navigation and the slave inertial navigation are on the same carrier, it can be considered $g_m \approx g_s = g$.

$$\begin{cases}\ddot{R}_m^i = C_m^i f_m^m - g \\ \ddot{R}_s^i = C_s^i f_s^s - g\end{cases} \tag{6}$$

Substituting (6) into (5) gives:

$$\begin{aligned}&C_s^i f_s^s - g = C_m^i f_m^m - g + C_m^i[\omega_{im}^m\times][\omega_{im}^m\times]R_{ms}^m \\ &+C_m^i[\dot{\omega}_{im}^m\times]R_{ms}^m + 2C_m^i[\omega_{im}^m\times]\dot{R}_{ms}^m + C_m^i\ddot{R}_{ms}^m\end{aligned} \tag{7}$$

Simplification gives:

$$\begin{aligned}C_s^i f_s^s &= C_m^i f_m^m + C_m^i[\omega_{im}^m\times][\omega_{im}^m\times]R_{ms}^m + \\ &C_m^i[\dot{\omega}_{im}^m\times]R_{ms}^m + 2C_m^i[\omega_{im}^m\times]\dot{R}_{ms}^m + C_m^i\ddot{R}_{ms}^m\end{aligned} \tag{8}$$

Multiplying C_i^s both sides of (8) at the same time, we can get:

$$\begin{aligned}f_s^s &= C_m^s f_m^m + C_m^s[\omega_{im}^m\times][\omega_{im}^m\times]R_{ms}^m + \\ &C_m^s[\dot{\omega}_{im}^m\times]R_{ms}^m + 2C_m^s[\omega_{im}^m\times]\dot{R}_{ms}^m + C_m^s\ddot{R}_{ms}^m\end{aligned} \tag{9}$$

The shift deformation between the MINS and the SINS can be divided into static shift deformation and dynamic shift deformation. Static shift deformation refers to the part that does not change for a long time, while dynamic line deformation is the part that changes all the time under the influence of environmental factors, expressed as:

$$R_{ms}^m = R_0^m + R_d^m \tag{10}$$

where R_0^m is the static shift deformation and R_d^m is the dynamic shift deformation, and the corresponding time differential is:

$$\begin{cases}\dot{R}_{ms}^m = \dot{R}_d^m \\ \ddot{R}_{ms}^m = \ddot{R}_d^m\end{cases} \tag{11}$$

Put (10), (11) into (9) to get:

$$\begin{aligned}f_s^s &= C_m^s[f_m^m + ([\omega_{im}^m\times][\omega_{im}^m\times] + [\dot{\omega}_{im}^m\times])R_0^m + \\ &([\omega_{im}^m\times][\omega_{im}^m\times] + [\dot{\omega}_{im}^m\times])R_d^m + 2[\omega_{im}^m\times]\dot{R}_d^m + \ddot{R}_d^m]\end{aligned} \tag{12}$$

When the Euler angle φ is a small angle,

$$C_m^s = I - [\varphi\times] \tag{13}$$

Substituting equation (13) into equation (12) can get:

$$\begin{aligned}f_s^s &= (I-[\varphi\times])[f_m^m + ([\omega_{im}^m\times][\omega_{im}^m\times] + [\dot{\omega}_{im}^m\times])R_0^m \\ &+([\omega_{im}^m\times][\omega_{im}^m\times] + [\dot{\omega}_{im}^m\times])R_d^m + 2[\omega_{im}^m\times]\dot{R}_d^m + \ddot{R}_d^m] \\ &= f_m^m + ([\omega_{im}^m\times][\omega_{im}^m\times] + [\dot{\omega}_{im}^m\times])R_0^m + ([\omega_{im}^m\times][\omega_{im}^m\times] \\ &+[\dot{\omega}_{im}^m\times])R_d^m + 2[\omega_{im}^m\times]\dot{R}_d^m + \ddot{R}_d^m - [\varphi\times]f_m^m - \\ &[\varphi\times][([\omega_{im}^m\times][\omega_{im}^m\times] + [\dot{\omega}_{im}^m\times])R_0^m + \\ &([\omega_{im}^m\times][\omega_{im}^m\times] + [\dot{\omega}_{im}^m\times])R_d^m + 2[\omega_{im}^m\times]\dot{R}_d^m + \ddot{R}_d^m]\end{aligned} \tag{14}$$

where R_d^m and φ both are small quantities, ignoring the second-order small quantity, we can get:

$$\begin{aligned}f_s^s - f_m^m &= (I-[\varphi\times])([\omega_{im}^m\times][\omega_{im}^m\times] + [\dot{\omega}_{im}^m\times])R_0^m \\ &+([\omega_{im}^m\times][\omega_{im}^m\times] + [\dot{\omega}_{im}^m\times])R_d^m + 2[\omega_{im}^m\times]\dot{R}_d^m + [f_m^m\times]\varphi\end{aligned} \tag{15}$$

The condition for this equation to measure the dynamic shift deformation is to know the static shift deformation and deformation angle, and at the same time require sufficient specific force observations, this equation cannot measure the dynamic shift deformation during static or uniform motion.

B. Angular velocity matching equation

As shown in Fig. 1, the angular velocity ω_{im}^m measured by the MINS is the projection of angular velocity of the m-frame relative to i-frame the in the m-frame, and the angular velocity ω_{is}^s measured from the SINS is the projection of the s-frame relative to the i-frame in the s-frame. Their relationship is expressed as:

$$\begin{aligned}\omega_{is}^s &= C_m^s(\omega_{im}^m + \omega_{ms}^m) \\ &= C_m^s\omega_{im}^m + \omega_{ms}^s\end{aligned} \tag{16}$$

where ω_{ms}^s is the projection of the angular velocity of the m-frame relative to the s-frame under the s-frame. When the deformation angle φ is a small angle, it can be considered as:

$$\begin{cases}\omega_{ms}^s = \dot{\varphi} \\ C_m^s = I - [\varphi\times]\end{cases} \tag{17}$$

Substituting (17) into (16) gives:

$$\omega_{is}^s = (I-[\varphi\times])\omega_{im}^m + \dot{\varphi} \tag{18}$$

The deformation angle φ can be divided into static angle deformation φ_0 and dynamic angle deformation θ,

$$\begin{cases}\varphi = \varphi_0 + \theta \\ \dot{\varphi} = \dot{\theta}\end{cases} \tag{19}$$

Put (19) into (18) to get:

$$\omega_{is}^s - \omega_{im}^m = \omega_{im}^m \times (\varphi_0 + \theta) + \dot{\theta} \tag{20}$$

The equation needs to know the static angle deformation when measuring the dynamic angle deformation, but when the carrier does not rotate enough and the angular velocity observation is insufficient, the equation cannot measure the dynamic angle deformation.

C. Velocity matching equation

The projection of (1) under the e-frame is:

$$R_s^e = R_m^e + R_{ms}^e = R_m^e + C_m^e R_{ms}^m \tag{21}$$

For (21) both sides relative to the e-frame time derivative can be obtained:

$$\begin{aligned} \dot{R}_s^e &= \dot{R}_m^e + C_m^e \dot{R}_{ms}^m + \dot{C}_m^e R_{ms}^m \\ &= \dot{R}_m^e + C_m^e \dot{R}_{ms}^m + C_m^e \omega_{em}^m \times R_{ms} \end{aligned} \tag{22}$$

Where $\dot{R}_s^e = v_s^e$, $\dot{R}_m^e = v_m^e$, (22) can be written as:

$$v_s^e = v_m^e + C_m^e \omega_{em}^m \times R_{ms} + C_m^e \dot{R}_d^m \tag{23}$$

Project the (23) to the n-frame:

$$v_s^n = v_m^n + C_m^n \omega_{em}^m \times R_{ms} + C_m^n \dot{R}_d^m \tag{24}$$

According to (10), (24) can be written as:

$$v_s^n = v_m^n + C_m^n \omega_{em}^m \times R_0 + C_m^n \omega_{em}^m \times R_d + C_m^n \dot{R}_d^m \tag{25}$$

Equation (25) can measure the static shift deformation when there are enough velocity observations and angular velocity observations.

D. Attitude angle matching equation

Let the attitude matrix measured by the main inertial navigation and the slaver inertial navigation be C_m^n and $C_s^{n'}$, The attitude transformation matrix between the MINS and SINS is C_m^s, and its expression is:

$$C_m^s = C_s^{n'T} C_n^{n'} C_m^n \tag{26}$$

Where $C_n^{n'}$ is the inconsistency of the navigation coordinate system caused by the two inertial navigation measurement errors, and the angle deviation ψ_ε is a small angle, then:

$$C_n^{n'} = I - [\psi_\varepsilon \times] \tag{27}$$

Then (26) can be written as;

$$C_m^s = C_s^{n'T} C_m^n - C_s^{n'T} [\psi_\varepsilon \times] C_m^n \tag{28}$$

Since C_m^n and $C_s^{n'}$ are very close and ψ_ε are small angles, according to the antisymmetric matrix similarity equation, the (28) can be written as:

$$C_m^s = C_s^{n'T} C_m^n - [\psi^n{}_\varepsilon \times] \tag{29}$$

ψ_ε^n is the projection of ψ_ε under the n-frame, when the deformation angle is a small angle, the equation (28) can be written as:

$$[\varphi \times] = I - C_s^{n'T} C_m^n + [\psi^n{}_\varepsilon \times] \tag{30}$$

C_m^n and $C_s^{n'}$ are the attitude measurement output of the two INSs, denote:

$$C_s^{n'T} C_m^n = \begin{bmatrix} C_{11} & C_{12} & C_{13} \\ C_{21} & C_{22} & C_{23} \\ C_{31} & C_{32} & C_{33} \end{bmatrix} \tag{31}$$

Then the angle deformation can be written as:

$$\varphi = [C_{32} + \psi^n{}_{\varepsilon_x} \quad C_{13} + \psi^n{}_{\varepsilon_y} \quad C_{21} + \psi^n{}_{\varepsilon_z}]^T = C_\varphi + \psi_\varepsilon^n \tag{32}$$

Where $C_\varphi = [C_{32} \quad C_{13} \quad C_{21}]^T$.

Equation (32) illustrates that the static angle deformation between two inertial navigation coordinate systems can be determined through the attitude measurements of the two Inertial Navigation Systems (INSs). When the carrier is stationary, the INS can still measure the carrier's attitude, enabling the equation to measure two static angle deformations between INSs.

From equations (15), (20), (25), and (32), it is evident that the velocity matching equation and the attitude matching equation can be utilized to measure the static angle deformation and static shift deformation of the two INSs. Notably, the velocity matching equation requires angular velocity observations, and static shift deformation cannot be measured under static conditions. However, the specific force matching equation can gauge static shift deformation by considering the relationship between static angle deformation and static shift deformation. Knowing the static angle deformation and static shift deformation allows the angular velocity matching equation and the specific force matching equation to measure dynamic angle deformation and dynamic shift deformation. These four inertial matching measurement equations exhibit complementary functions. Consequently, the multi-vector inertial matching measurement method, combined with these equations, enhances the robustness of deformation matching and extends the measurement range.

Nevertheless, the angular velocity matching equation necessitates angular velocity observations, and the specific force matching equation requires acceleration observations. During carrier motion, the simultaneous occurrence of rotational motion and acceleration motion cannot be guaranteed, resulting in the inability to measure dynamic angular deformation and dynamic shift deformation simultaneously. Therefore, a conversion relationship between angular deformation and shift deformation is required.

III. RELATIONSHIP BETWEEN ANGLE DEFORMATION AND SHIFT DEFORMATION

During the hull deformation process, angular deformation and shift deformation are not independent but are mutually constrained. The high stiffness of ship materials makes it challenging for the hull to experience substantial stretching and compression. Instead, deformation and angular deformation primarily result from the twisting deformation of the hull. Consequently, when the hull undergoes bending deformation, simultaneous angular deformation and shift deformation occur. Fig.2 illustrates an example where the hull deforms in the pitch direction, and the corresponding shift deformation between the master and slave inertial navigation systems changes accordingly.

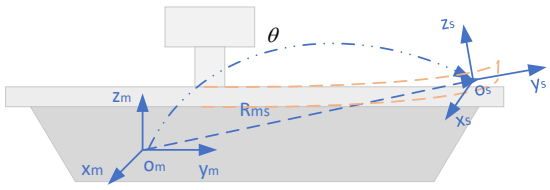

Fig. 2. The hull undergoes both angular and shift deformations

Assuming that the static shift between the MINS and the SINS of the hull is $R_0^m = [r_{x_0}, r_{y_0}, r_{z_0}]$, the static deformation angle is a small angle, and the dynamic deformation angle is $\theta = [\theta_x, \theta_y, \theta_z]$, in order to simplify the analysis, take the OYZ-plane as an example, as shown in Fig. 3

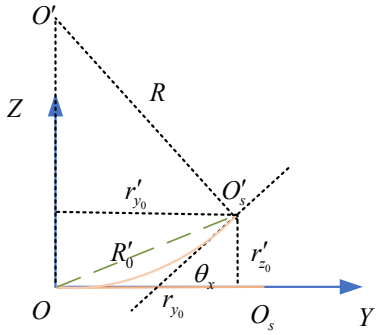

Fig. 3. Angular and shift deformations on the OYZ - plane

The deck of the ship OO_s, whose length is r_{y_0}, is affected by external factors, and the deck is bent and deformed, and the bending is an arc OO'_s, and the bending angle is θ_x, In this case the shift deformation becomes $R'_0=[r_{x_0},r'_{y_0},r'_{z_0}]$, Due to the strong structural stiffness, the tension and compression of the deck is negligible, so the length of the arc OO'_s is still r_{y_0}, and the radius of the circle corresponding to the arc OO'_s is R , the angle $\angle OO'O'_s$ is θ_x,

$$\begin{cases} R=\dfrac{r_{y_0}}{\theta_x} \\ r'_{y_0}=R\sin\theta_x \\ r'_{z_0}=R(1-\cos\theta_x) \end{cases} \tag{33}$$

Equation (33) can be sorted out to get:

$$\begin{cases} r'_{y_0}=\dfrac{r_{y_0}\sin\theta_x}{\theta_x} \\ r'_{z_0}=\dfrac{r_{y_0}(1-\cos\theta_x)}{\theta_x} \end{cases} \tag{34}$$

Similarly, the deformation caused by θ_y is:

$$\begin{cases} r'_{z_0}=\dfrac{r_{z_0}\sin\theta_y}{\theta_y} \\ r'_{x_0}=\dfrac{r_{z_0}(1-\cos\theta_y)}{\theta_y} \end{cases} \tag{35}$$

The deformation caused by θ_z is:

$$\begin{cases} r'_{x_0}=\dfrac{r_{x_0}\sin\theta_z}{\theta_z} \\ r'_{y_0}=\dfrac{r_{x_0}(1-\cos\theta_z)}{\theta_z} \end{cases} \tag{36}$$

Taken together, the shift deformation caused by the angle deformation $\theta=[\theta_x,\theta_y,\theta_z]$ is:

$$\begin{cases} r'_{x_0}=\dfrac{r_{x_0}\sin\theta_z}{\theta_z}+\dfrac{r_{z_0}(1-\cos\theta_y)}{\theta_y} \\ r'_{y_0}=\dfrac{r_{y_0}\sin\theta_x}{\theta_x}+\dfrac{r_{x_0}(1-\cos\theta_z)}{\theta_z} \\ r'_{z_0}=\dfrac{r_{z_0}\sin\theta_y}{\theta_y}+\dfrac{r_{y_0}(1-\cos\theta_x)}{\theta_x} \end{cases} \tag{37}$$

Taylor expansion of the coefficients can be obtained:

$$\begin{cases} \dfrac{\sin\theta}{\theta}=1-\dfrac{\theta^2}{6}+o(\theta) \\ \dfrac{1-\cos\theta}{\theta}=\dfrac{\theta}{2}-\dfrac{\theta^3}{24}+o(\theta) \end{cases} \tag{38}$$

According to Taylor expansion, (36) can be rewritten as:

$$\begin{cases} r'_{x_0}=r_{x_0}(1-\dfrac{\theta_z^{\,2}}{6}+o(\theta_z))+r_{z_0}(\dfrac{\theta_y}{2}-\dfrac{\theta_y^{\,3}}{24}+o(\theta_y)) \\ r'_{y_0}=r_{y_0}(1-\dfrac{\theta_x^{\,2}}{6}+o(\theta_x))+r_{x_0}(\dfrac{\theta_z}{2}-\dfrac{\theta_z^{\,3}}{24}+o(\theta_z)) \\ r'_{z_0}=r_{z_0}(1-\dfrac{\theta_y^{\,2}}{6}+o(\theta_y))+r_{y_0}(\dfrac{\theta_x}{2}-\dfrac{\theta_x^{\,3}}{24}+o(\theta_x)) \end{cases} \tag{39}$$

Ignoring higher-order small quantities the (38) can be rewritten as:

$$\begin{cases} r'_{x_0}=r_{x_0}(1-\dfrac{\theta_z^{\,2}}{6})+\dfrac{r_{z_0}\theta_y}{2} \\ r'_{y_0}=r_{y_0}(1-\dfrac{\theta_x^{\,2}}{6})+\dfrac{r_{x_0}\theta_z}{2} \\ r'_{z_0}=r_{z_0}(1-\dfrac{\theta_y^{\,2}}{6})+\dfrac{r_{y_0}\theta_x}{2} \end{cases} \tag{40}$$

Written in matrix form as:

$$R'_0=R_0^m+A_0\theta \tag{41}$$

Where the matrix A_0 is:

$$A_0=\frac{1}{2}\begin{bmatrix} 0 & r_{z_0} & 0 \\ 0 & 0 & r_{x_0} \\ r_{y_0} & 0 & 0 \end{bmatrix} \tag{42}$$

According to (10), it can be known that the dynamic shift deformation is:

$$R_d^m=A_0\theta \tag{43}$$

According to (43), it can be seen that when the deformation angle is a small angle, there is approximately a linear relationship between the dynamic shift deformation and the dynamic deformation angle.

IV. Deformation Measurement Based on Multi-Vector Matching

Owing to errors in the angular velocity, attitude, specific force and velocity measured by INS, it is necessary to improve the accuracy of measurement by filtering. From (15), (20), (25), (32), (43), it can be seen that the measurement equation is a linear equation, so the Kalman filter method can

be used to improve the measurement accuracy.

A. Hull dynamic deformation model

According to the description in [15], the dynamic deformation angle $\theta=[\theta_x,\theta_y,\theta_z]^T$ can be described by a second-order Markov process, and the specific equation is:

$$\ddot{\theta}_i+2\mu_{\theta_i}\dot{\theta}_i+b_{\theta_i}{}^2\theta_i=2b_{\theta_i}\sqrt{D_{\theta_i}\mu_{\theta_i}}w_\theta(t) \quad (44)$$

where $i=x,y,z$ are the three axes, $b_{\theta_i}{}^2=\mu_{\theta_i}{}^2+\lambda_{\theta_i}{}^2$, μ_{θ_i} is the irregularity coefficient, and λ_{θ_i} is the main frequency of dynamic deformation, D_{θ_i} is a constant coefficient and $w_\theta(t)$ is white noise.

According to the (43), the dynamic shift deformation $R_d^m=[R_{d_x}^m,R_{d_y}^m,R_{d_z}^m]^T$ can also be described by a second-order Markov process, and the equation is:

$$\ddot{R}_{d_i}^m+2\mu_{R_i}\dot{R}_{d_i}^m+b_{R_i}{}^2R_{di}^m=2b_{R_i}\sqrt{D_{R_i}\mu_{R_i}}w_R(t) \quad (45)$$

Where $i=x,y,z$ are the three axes, $b_{R_i}{}^2=\mu_{R_i}{}^2+\lambda_{R_i}{}^2$, μ_{R_i} is the irregularity coefficient, and λ_{R_i} is the main frequency of dynamic deformation, D_{R_i} is a constant coefficient and $w_R(t)$ is white noise.

The static angle deformation and static shift deformation can be considered as constant values in the short term, so $\dot{\varphi}_0=0$.

B. Errors of gyroscope and accelerometer

The error of laser gyro ε in inertial navigation is divided into constant error $\varepsilon_0=[\varepsilon_{0_x},\varepsilon_{0_y},\varepsilon_{0_z}]^T$ and random error $\varepsilon_r=[\varepsilon_{r_x},\varepsilon_{r_y},\varepsilon_{r_z}]^T$, the constant error is a constant, and the random error is white noise. Similarly, the accelerometer error ε' in inertial navigation is also divided into constant error and random error, the random error is white noise.

C. System state equation

The state vector of the hull deformation measurement system is:

$$X=[\varphi_0\quad\theta\quad\dot{\theta}\quad R_0^m\quad R_d^m\quad\dot{R}_d^m\quad\Delta\varepsilon\quad\Delta\varepsilon']^T \quad (46)$$

Where $\varphi_0=[\varphi_{0_x}\quad\varphi_{0_y}\quad\varphi_{0_z}]^T$ is the static angle deformation, $\theta=[\theta_x\quad\theta_y\quad\theta_z]^T$ is the dynamic angle deformation, $\dot{\theta}=[\dot{\theta}_x\quad\dot{\theta}_y\quad\dot{\theta}_z]^T$ is the time differential of θ, $R_0^m=[R_{0_x}^m\quad R_{0_y}^m\quad R_{0_z}^m]^T$ is the static shift deformation, $R_d^m=[R_{d_x}^m\quad R_{d_y}^m\quad R_{d_z}^m]^T$ is the dynamic shift deformation, $\dot{R}_d^m=[\dot{R}_{d_x}^m\quad\dot{R}_{d_y}^m\quad\dot{R}_{d_z}^m]^T$ is the time differential of R_d^m, and $\Delta\varepsilon=[\Delta\varepsilon_x\quad\Delta\varepsilon_y\quad\Delta\varepsilon_z]^T$ is the difference between the gyro errors of the two INSs, which can be regarded as white noise , $\Delta\dot{\varepsilon}=[\Delta\dot{\varepsilon}_x\quad\Delta\dot{\varepsilon}_y\quad\Delta\dot{\varepsilon}_z]^T$ for $\Delta\varepsilon$ the time differential of , satisfying the equation:

$$\Delta\dot{\varepsilon}_i+\mu_i'\Delta\varepsilon_i=\sigma_i\sqrt{2\mu_i'}w(t) \quad (47)$$

where μ_i' is the irregular coefficient, σ_i is the standard deviation of the random error, $w(t)$ is white noise.

$\Delta\varepsilon'=[\Delta\varepsilon_x'\quad\Delta\varepsilon_y'\quad\Delta\varepsilon_z']^T$ is the difference between the accelerometer errors of the INSs, and $\Delta\dot{\varepsilon}'=[\Delta\dot{\varepsilon}_x'\quad\Delta\dot{\varepsilon}_y'\quad\Delta\dot{\varepsilon}_z']^T$ is the time differential of $\Delta\varepsilon'$, satisfying the equation:

$$\Delta\dot{\varepsilon}_i'+\mu_i''\Delta\varepsilon_i'=\sigma_i'\sqrt{2\mu_i''}w'(t) \quad (48)$$

where μ_i'' is the irregular coefficient, σ_i' is the standard deviation of the random error, $w'(t)$ is white noise.

The matrix form of the state equation of the system can be obtained:

$$\dot{X}=FX+Gw \quad (49)$$

Where

$$F=\begin{bmatrix}0_{3\times3}&0_{3\times3}&0_{3\times3}&0_{3\times3}&0_{3\times3}&0_{3\times3}&0_{3\times3}&0_{3\times3}\\0_{3\times3}&0_{3\times3}&I_{3\times3}&0_{3\times3}&0_{3\times3}&0_{3\times3}&0_{3\times3}&0_{3\times3}\\0_{3\times3}&B_0&B_1&0_{3\times3}&0_{3\times3}&0_{3\times3}&0_{3\times3}&0_{3\times3}\\0_{3\times3}&0_{3\times3}&0_{3\times3}&0_{3\times3}&0_{3\times3}&0_{3\times3}&0_{3\times3}&0_{3\times3}\\0_{3\times3}&0_{3\times3}&0_{3\times3}&0_{3\times3}&I_{3\times3}&0_{3\times3}&0_{3\times3}&0_{3\times3}\\0_{3\times3}&0_{3\times3}&0_{3\times3}&0_{3\times3}&B_2&B_2&0_{3\times3}&0_{3\times3}\\0_{3\times3}&0_{3\times3}&0_{3\times3}&0_{3\times3}&0_{3\times3}&0_{3\times3}&B_4&0_{3\times3}\\0_{3\times3}&0_{3\times3}&0_{3\times3}&0_{3\times3}&0_{3\times3}&0_{3\times3}&0_{3\times3}&B_5\end{bmatrix},$$

$G=diag(0_{6\times6},C_0,0_{6\times6},C_1,C_2,C_3)$,

$B_0=diag(-b_{\theta_x}{}^2,-b_{\theta_y}{}^2,-b_{\theta_z}{}^2)$, $B_1=diag(-2\mu_{\theta_x},-2\mu_{\theta_y},-2\mu_{\theta_z})$

$B_2=diag(-b_{R_x}{}^2,-b_{R_y}{}^2,-b_{R_z}{}^2)$, $B_3=diag(-2\mu_{R_x},-2\mu_{R_y},-2\mu_{R_z})$

$B_4=diag(-\mu_x',-\mu_y',-\mu_z')$ $B_5=diag(-\mu_x'',-\mu_y'',-\mu_z'')$

$C_0=diag(2b_{\theta_x}\sqrt{D_{\theta_x}\mu_{\theta_x}},2b_{\theta_y}\sqrt{D_{\theta_y}\mu_{\theta_y}},2b_{\theta_z}\sqrt{D_{\theta_z}\mu_{\theta_z}})$,

$C_1=diag(2b_{R_x}\sqrt{D_{R_x}\mu_{R_x}},2b_{R_y}\sqrt{D_{R_y}\mu_{R_y}},2b_{R_z}\sqrt{D_{R_z}\mu_{R_z}})$,

$C_2=diag(\sigma_x\sqrt{2\mu_x'},\sigma_y\sqrt{2\mu_y'},\sigma_z\sqrt{2\mu_z'})$,

$C_3=diag(\sigma_x'\sqrt{2\mu_x''},\sigma_y'\sqrt{2\mu_y''},\sigma_z'\sqrt{2\mu_z''})$

D. System measurement equation

Considering the errors of gyroscope and accelerometer and the relationship between dynamic shift deformation and dynamic deformation angle, (15), (20), (25), (32) become:

$$\begin{cases}\omega_{is}^s-\omega_{im}^m=\omega_{im}^m\times(\varphi_0+\theta)+\dot{\theta}+\Delta\varepsilon\\f_s^s-f_m^m=([\omega_{im}^m\times][\omega_{im}^m\times]+[\dot{\omega}_{im}^m\times])R_0^m\\+([\omega_{im}^m\times][\omega_{im}^m\times]+[\dot{\omega}_{im}^m\times])R_d^m\\+2[\omega_{im}^m\times]\dot{R}_d^m+f_m^m\times(\varphi_0+\theta)+\Delta\varepsilon'\\v_s^n-v_m^n=C_m^n\omega_{em}^m\times R_0+C_m^n\omega_{em}^m\times R_d+C_m^n\dot{R}_d^m+w_v\\C_\varphi=\psi_\varepsilon^n-(\varphi_0+\theta)+w_c\end{cases} \quad (50)$$

Where the w_v and w_c is white noise.

Observations can be set as:

$$Z=\begin{bmatrix}\omega_{is}^s-\omega_{im}^m & f_s^s-f_m^m & v_s^n-v_m^n & C_\varphi\end{bmatrix} \quad (51)$$

According to (50), the corresponding observation equation

can be obtained as:

$$Z = HX + v \tag{52}$$

Where

$$H = \begin{bmatrix} \omega_{im}^m \times & \omega_{im}^m \times & I_{3\times3} & 0_{3\times3} & 0_{3\times3} & 0_{3\times3} & I_{3\times3} & 0_{3\times3} \\ f_m^m \times & f_m^m \times & 0_{3\times3} & D & D & 2[\omega_{im}^m \times] & 0_{3\times3} & I_{3\times3} \\ 0_{3\times3} & 0_{3\times3} & 0_{3\times3} & C_m^n \omega_{em}^m \times & C_m^n \omega_{em}^m \times & C_m^n & 0_{3\times3} & 0_{3\times3} \\ -I_{3\times3} & -I_{3\times3} & 0_{3\times3} & 0_{3\times3} & 0_{3\times3} & 0_{3\times3} & 0_{3\times3} & 0_{3\times3} \end{bmatrix}$$

$$, \ D = [\omega_{im}^m \times][\omega_{im}^m \times] + \dot{\omega}_{im}^m \times$$

The error v is:

$$v = \begin{bmatrix} 0_{3\times3} & 0_{3\times3} & w_v & w_c \end{bmatrix}^T \tag{53}$$

V. EXPERIMENTAL VERIFICATION AND RESULT ANALYSIS

The method proposed in this paper is validated using laser Inertial Navigation Systems (INSs) on a simulation device in the laboratory. And compare it with the original angular velocity vector matching measurement method. For simplicity, the two methods are abbreviated as MVM(multi-vector matching measurement method) and AVM(velocity vector matching measurement method), respectively.

A. Test environment

The experimental setup involves using a 5-meter-long elastic steel plate to replicate the hull's deck. The steel plate is compressed to simulate deck deformation, and a deformation measurement system is arranged on the device to validate the proposed method in this paper. The MINS is positioned in the middle, with the SINS located 2 meters away from the MINS. The centers of both INSs are aligned with the central axis of the device. To measure the actual deformation and verify the accuracy of the deformation measurement system, a photoelectric autocollimator is placed on one side of the device. The specific measurement environment is illustrated in Fig.9.

Fig. 4. Deformation measurement test environment

B. Test results

During the test, external force impacts occur at intervals of 5 minutes, with each impact lasting for a duration of 1 hour. Data from the photoelectric autocollimator and inertial navigation are recorded separately. Utilizing the recorded inertial navigation data, the structure's deformation is calculated using both the angular velocity matching method and the multi-vector matching method. The results are depicted in the Fig.10. To assess measurement accuracy, a comparison is made between the roll angle deformation measured by the photoelectric autocollimator and the roll angle deformation measured by the multi-vector inertial matching, as presented in Table V.

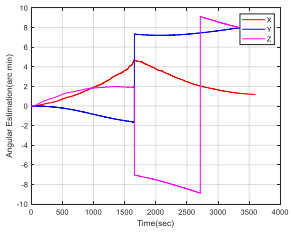

Fig. 5. AVM measurement deformation

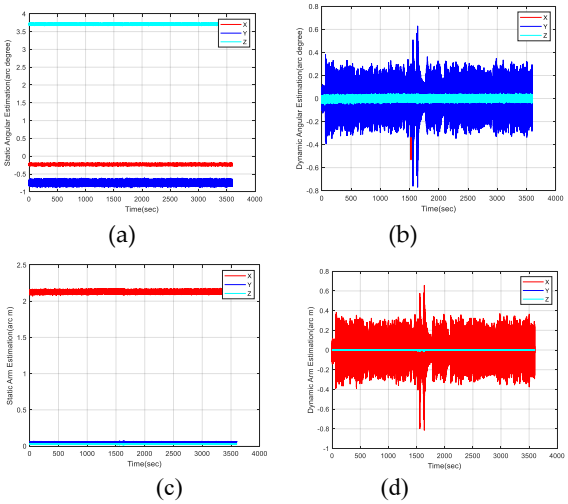

(a) (b) (c) (d)

Fig. 6. MVM measurement deformation. (a) Static angle deformation. (b) Dynamic angle deformation (c) Static shift deformation. (d) Dynamic shift deformation

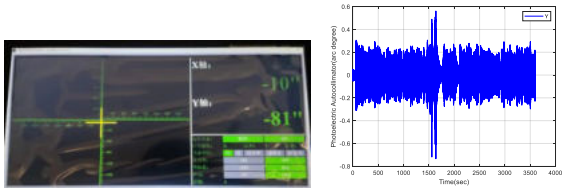

(a) (b)

Fig. 7. Photoelectric autocollimator test results. (a) The photoelectric autocollimator. (b) The test results.

TABLE I. DEFORMATION ESTIMATION (DEG/M)

Method	*Estimation*	*X*	*Y*	*Z*
MVM	Static angle	\	0.0071	\
AVM	static shift	\	\	\

Fig. 5 illustrates that the angular velocity matching measurement method remains ineffective in measuring deformation when there is only a small roll. In contrast, Fig. 6 demonstrates that the multi-vector inertial matching measurement algorithm proposed in this paper performs better in actual conditions, effectively measuring the entire deformation between the two inertial navigation coordinate systems. Both Fig. 7 and Table I confirm that the measurement accuracy of the multi-vector inertial matching deformation measurement method can essentially reach a measurement accuracy of 20 arcsec.

The above experimental results show that the deformation measurement method based on multi-vector inertia matching proposed in this paper has better robustness. When the carrier is at rest, it can provide more observations than the traditional inertia matching method, and thus the deformation can be measured. At the same time, the method proposed in this

paper is able to measure the shift deformation and thus has a better scope of application.

VI. Conclusion

This paper introduces a novel approach, the multi-vector inertial matching measurement method, developed after analyzing various inertial matching equations. Addressing the limitation of existing methods in measuring deformation under static conditions, this proposed method leverages the unique characteristics of each equation. Notably, it not only successfully measures deformation in a static environment but also captures shift deformation between two Inertial Navigation Systems (INSs). Moreover, the method overcomes the original limitation of measuring shift deformation, providing a comprehensive solution.

Given the challenging conditions for dynamic shift deformation measurement, this paper introduces a dynamic deformation conversion relationship. This innovation allows the proposed method to measure dynamic shift deformation even when the force vector observation is not apparent. Testing methods validate the effectiveness of the multi-vector inertial matching measurement method in measuring deformation under static conditions, as well as capturing outgoing shift deformation and angular deformation under dynamic conditions.

Comparative analysis with the original angular velocity matching deformation measurement method demonstrates the superior stability and broader applicability of the multi-vector inertial matching measurement method. While these findings are promising, further validation is required, particularly in real sea conditions. Therefore, the feasibility of this method needs to be confirmed through verification on sailing ships in future studies.

References

[1] Li, Y., Wang, D., and Tong, J. (2022) A hull deformation measurement method based on fiber optic gyro angular rate matching in complex sea conditions. Proceedings of the Institution of Mechanical Engineers, Part M: Journal of Engineering for the Maritime Environment. 236 (1), 34–47.

[2] Shortelle, K.J., Graham, W.R., and Rabourn, C. (1998) F-16 flight tests of a rapid transfer alignment procedure. in: IEEE 1998 Position Location and Navigation Symposium (Cat. No.98CH36153), IEEE, Palm Springs, CA, USApp. 379–386.

[3] Chang, L. and Hu, B. (2018) Robust Initial Attitude Alignment for SINS/DVL. IEEE/ASME Transactions on Mechatronics. 23 (4), 2016–2021.

[4] Xu, D., Zhang, X., Peng, X., Yang, G., and Chen, J. (2022) An anti-vibration-shock inertial matching measurement method for hull deformation. IET Signal Processing. 16 (4), 490–500.

[5] Zhang, Y., Yang, S., Qin, S., Hu, F., and Wu, W. (2018) A New Bias Error Prediction Model for High-Precision Transfer Alignment. Sensors. 18 (10), 3277.

[6] Yang, D., Wang, S., Li, H., Liu, Z., and Zhang, J. (2013) Performance Enhancement of Large-Ship Transfer Alignment: A Moving Horizon Approach. Journal of Navigation. 66 (1), 17–33.

[7] Gebre-Egziabher, D. and Shao, Y. (2010) Model for JPALS/SRGPS Flexure and Attitude Error Allocation. IEEE Transactions on Aerospace and Electronic Systems. 46 (2), 483–495.

[8] Wang, B., Deng, Z., Liu, C., Xia, Y., and Fu, M. (2014) Estimation of Information Sharing Error by Dynamic Deformation Between Inertial Navigation Systems. IEEE Transactions on Industrial Electronics. 61 (4), 2015–2023.

[9] Liu, H., Sun, C., Zhang, Y., Liu, X., Liu, J., Zhang, X., et al. (2015) Hull deformation measurement for spacecraft TT&C ship by Photogrammetry. Science China Technological Sciences. 58 (8), 1339–1347.

[10] Petovello, Mark.G., O'Keefe, K., Lachapelle, G., and Cannon, M.E. (2009) Measuring Aircraft Carrier Flexure in Support of Autonomous Aircraft Landings. IEEE Transactions on Aerospace and Electronic Systems. 45 (2), 523–535.

[11] Sun, F., Guo, C., Gao, W., and Li, B. (2007) A New Inertial Measurement Method of Ship Dynamic Deformation. in: 2007 International Conference on Mechatronics and Automation, IEEE, Harbin, Chinapp. 3407–3412.

[12] He, Y., Zhang, X., and Peng, X. (2018) A Model-Free Hull Deformation Measurement Method Based on Attitude Quaternion Matching. 6 6. https://doi.org/10.1109/access.2018.2807183

[13] Mochalov, A.V. and Kazantsev, A.V. (2002) Use of ring laser units for measurement of moving object deformations. in: V.E. Privalov (Ed.), St. Petersburg, Russiap. 85. https://doi.org/10.1117/12.454660

[14] Wu, W., Chen, S., and Qin, S. (2012) Determination of dynamic flexure model parameters for ship angular deformation measurement. in: Proceedings of 2012 UKACC International Conference on Control, IEEE, Cardiff, United Kingdompp. 964–969.

[15] Wu, W., Qin, S., and Chen, S. (2013) Coupling influence of ship dynamic flexure on high accuracy transfer alignment. International Journal of Modelling, Identification and Control. 19 (3), 224.

[16] Xu, B., Duan, T., and Wang, Y. (2017) An inertial measurement method of ship deformation based on IMM filtering. Optik. 140 601–609.

[17] Li, D., Ma, X., and Wang, Y. (2018) Using Accelerometers Enhance Measurement Performance of Hull Deformation. in: 2018 Chinese Automation Congress (CAC), IEEE, Xi'an, Chinapp. 2346–2352.

[18] [18] Ma, X., Qin, S., Wang, X., Wu, W., Zheng, J., and Pan, Y. (2017) Hull Structure Monitoring Using Inertial Measurement Units. IEEE Sensors Journal. 17 (9), 2676–2681